Available online at www.sciencedirect.com
ScienceDirect
Journal of the European Ceramic Society 30 (2010) 2643–2652
www.elsevier.com/locate/jeurceramsoc

Thermal stress relaxation creep and microstructural evolutions of nanostructured SiC ceramics by liquid phase sintering

Kazuya Shimoda [a,b,*], Sosuke Kondo [a], Tatsuya Hinoki [a], Akira Kohyama [a,c]

[a] *Institute of Advanced Energy, Kyoto University, Gokasho Uji, Kyoto 611-0011, Japan*
[b] *DEN/DANS/DMN/SRMA, CEA-Saclay, Gif-sur-Yvette Cedex 91191, France*
[c] *Department of Material Science and Engineering, Muroran Institute of Technology, 27-1 Mizumoto-cho, Muroran 050-8585, Japan*

Received 19 January 2010; received in revised form 8 April 2010; accepted 23 April 2010
Available online 31 May 2010

Abstract

We explored the thermal relaxation creep characteristics of nanostructured SiC ceramics by bend stress relaxation (BSR) method. The effects of the differences in microstructure and secondary phases by liquid phase sintering at 1800 or 1900 °C were especially discussed, based on microstructural evolutions during the creep. The creep was characterized by the BSR ratio (m) of ∼0.80 up to 1200 °C, and the proportion of amorphous phase as a secondary phase was related to the creep resistance at 1300 °C. The microstructural evolutions during the creep consisted firstly in the re-distribution of amorphous phase, probably as a consequence of its viscous flow, and secondly in an extensive nucleation and growth of cavities. Furthermore, the former enhanced inter-diffusion of Al–Y among intergranular areas above the ternary eutectic temperature, which caused the significantly reduced creep resistance, and the latter reflected the crystalline YAG decomposition as another secondary phase near 1500 °C.

Keywords: Sintering; SiC; Creep; Microstructural evolution

1. Introduction

Silicon carbide (SiC) offers many advantages, such as low specific weight, excellent high-temperature strength, high resistance to corrosion, oxidation and wear, good relative thermal conductivity, relatively low coefficient of thermal expansion and good behaviors under irradiation (inherent low radioactivity, low neutron absorption and low irradiation swelling). This combination of unique properties makes SiC promising structural materials most frequently used for high-temperature[1,2] and/or nuclear[2–4] applications. SiC ceramics sintered with various oxide additives, so called liquid phase sintered SiC (LPS-SiC) ceramics, have become a significant class of structural materials for these applications. The additives promote the formation of a liquid phase at a relatively low temperature (1750–2000 °C), and densification occurs by liquid rearrangement and solution-precipitation. After cooling, the oxide remains as a secondary phase, located as pockets between multigrains and as thin films at intergranular grain boundaries, which significantly influence high-temperature mechanical properties of the materials. In particular, the oxide remains are anticipated to impose deleterious effects on the creep resistance.[5–7] Besides, major load to be imposed on structural materials is thermal stress for these applications. The stress relaxation behavior under deformation-controlled stress should be primarily clarified. A few types of test methods (i.e., compression,[5–7] tension,[8] torsion[9] and bend[10–13]) for evaluation of the thermal creep have been applied so far. Bend stress relaxation (BSR) method, which is one of bend type test techniques, has been originally developed for evaluation of creep properties of ceramic fibers.[11] Recently, Katoh et al. have developed the BSR technique of SiC bulk materials using thin-strip form, aiming at evaluation of the irradiation creep of the materials which were equivalent to the matrix in SiC/SiC composites.[12,13] In the last years, nanostructured LPS-SiC ceramics using SiC nano-powder as a starting material have been widely researched in the world because of its excellent performances on sinterability and mechanical properties.[14–16] However, the very fine grains derived from nano-powder enhance grain-boundary activity in SiC ceram-

* Corresponding author. Present address: DEN/DANS/DMN/SRMA, CEA-Saclay, Gif-sur-Yvette Cedex 91191, France. Tel.: +33 1 69 08 12 03; fax: +33 1 69 08 71 67.
E-mail address: kazuya.shimoda@cea.fr (K. Shimoda).

0955-2219/$ – see front matter © 2010 Elsevier Ltd. All rights reserved.
doi:10.1016/j.jeurceramsoc.2010.04.035

ics, thus creep of nanostructured LPS-SiC ceramics has to be evaluated.

This paper addresses the issue of thermal stress relaxation creep and microstructural evolutions during the creep of nanostructured LPS-SiC ceramics using SiC nano-powder as a starting material. In particular, correlations between the creep resistance and microstructural evolutions are discussed, focused on the secondary phase in pockets between multigrains and at intergranular grain boundaries. Finally, a mechanism is suggested to explain the BSR creep behavior of the LPS-SiC ceramics as a function of the test temperature.

2. Experimental procedure

2.1. Materials

β-SiC nano-powder with sintering additives of 5.4 wt% Al_2O_3, 3.6 wt% Y_2O_3 and 3 wt% SiO_2 was hot-pressed at 1800 or 1900 °C under a pressure of 20 MPa for 1 h in Ar atmosphere. The starting nano-powder had a mean grain size of 50 nm, produced by the plasma-enhanced chemical vapor deposition (PECVD) method (T-1 grade, Sumitomo-Osaka Cement Co. Ltd., Tokyo, Japan). Characterizations of the starting nano-powder employed in this study were previously reported in detail.[17] The formation temperature of a transient eutectic phase between Al_2O_3 and Y_2O_3 can be lowered by including a small amount of SiO_2, which leads to the attractive promotion of densification of SiC nano-powder below 1900 °C.[18] Polycrystalline chemically vapor-deposited SiC (CVD-SiC) ceramics (Roman and Haas Co., Waborn, MA, USA) were used for the examination of high-purity SiC with clean grain boundaries.

2.2. Bend stress relaxation (BSR) creep test

The thin-strip specimens with a dimension of $40^{W} \times 0.1^{L} \times 1.0^{T}$ mm^3 were mechanically prepared for BSR creep tests from hot-pressed samples. Fig. 1(a) shows a schematic illustration of the fixture design in this study, following the guidance by Katoh et al.[12] The fixtures with thin-strip specimens were placed in a carbon crucible, and then exposed at a temperature range of 1000–1500 °C. The all tests were exposed in commercially available high-purity Ar atmosphere (O_2 partial pressure: $P_{O_2} = \sim 0.1$ Pa). Three specimens for each test temperature were exposed with the heating rate of ~20 °C/min and the holding time of 0.5, 1 and 3 h. The furnace containing specimens was cooled by room temperature without control of the cooling rate. Holders were made from Hexoloy™ SA to avoid a potential interaction with SiC specimens at high temperatures. The specimen holders were designed to retain the thin-strip samples in a narrow gap with a curvature of 100 mm radius. Bend radius of the specimens was smallest in the center and largest at the both ends, but the variation was within ~10% over the specimen length except for the very end regions. The bend radius averaged over the entire specimens length was used to determine the residual stress after relaxation (σ_a) by the following Eq. (1):

$$\sigma_a = \frac{E_T t(\varphi_o - \varphi_a)}{2L} \quad (1)$$

where E_T is the Young's modulus, t is the specimen thickness, L is the specimens length, φ_o is the initial bend angle and φ_a is the residual bend angle in the freed sample. Hence, the BSR ratio (m) is given by the following Eq. (2):

$$m = \frac{\sigma_a}{\sigma_o} = \frac{1 - \varphi_a}{\varphi_o} \quad (2)$$

where σ_o is the initial stress. As shown in Fig. 1(b), the bend radii for individual specimens were determined by measuring the differential tangential angles by optical microscopy at both ends of the sample strips before and after. The accuracy in bend angle determination by digital optical microscopy was <0.1°. This gives the potential error of ~0.02 in the BSR ratio (m) determination in the present experimental configuration. The parameter m varies between 0 for complete stress relaxation and 1 for no stress relaxation.

2.3. Microstructural observation

The microstructural observations before and after the BSR tests were performed with JEOL JEM-2010 transmission electron microscope (TEM) and JEOL JEM-2200FS field emission transmission electron microscopy (FE-TEM). The energy dispersive X-ray spectroscopy (EDXS) system on the FE-TEM was utilized to investigate chemical changes in pockets between multigrains and at intergranular grain boundaries. The TEM and FE-TEM specimens were prepared utilizing a focused ion-beam (FIB) micro-processing device, in which thin-foils could be obtained on a carbon film supported by copper grids.

3. Results

3.1. Initial microstructural characterization of two LPS-SiC ceramics

Table 1 summarizes some densification and mechanical properties at room temperature of two LPS-SiC and CVD-SiC ceramics used in this study. After hot-pressing, two materials were well densified with excellent mechanical properties, such as bending strength over 800 MPa, Vicker's hardness over 26 GPa, and indentation fracture toughness over 4.7 MPa m$^{1/2}$. Fig. 2 shows the diffraction pattern measured with Cu Kα radiation (λ = 0.154 nm). The peak position clearly showed the existence of the β-SiC (3C) polytype (JCPDS No. 29-1129) and crystalline yttrium–aluminum garnet (YAG: $Al_5Y_3O_{12}$) (JCPDS No. 33-0040). The cubic polytype has the highest symmetry and, thus shows the lowest number of diffraction lines. All lower symmetric SiC polytypes present diffraction positions near to and between the positions of the β-SiC (3C) diffraction lines. However, no intensity was detected at the between position, e.g. at $2\theta = 34.2°$, 38.2°, 65.8° and 73.6° for α-SiC (6H). Al_2O_3–Y_2O_3 additive systems in LPS-SiC ceramics normally form crystalline YAG in pockets.[5–7,19–22] The sharper peak lines of YAG were

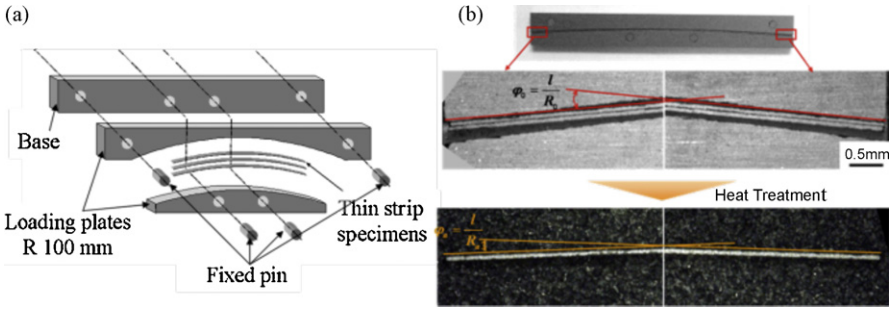

Fig. 1. (a) Illustration of the BSR creep fixture and (b) measurement of bend radius of constrained and relaxed thin-strip samples by optical microscopy.

Table 1
Densification and mechanical properties of two LPS-SiC and CVD-SiC ceramics used in this study.

Designation	Densification			Mechanical properties		
	Bulk density (g/cm^3)	Relative density (%)	Bending strength (MPa)	Young's modulus (GPa)	Vicker's Hardness (GPa)	Fracture toughness ($MPa\,m^{1/2}$)
LPS-SiC at 1800	3.05	94	818	351	26	4.8
LPS-SiC at 1900	3.11	97	829	371	27	4.7
CVD-SiC	3.19	99	789	460	25	3.3

found in LPS-SiC at 1900. However, two LPS-SiC ceramics had the difficulty to identify another phases from XRD, because the contents were under the detecting limit and/or because they present an amorphous structure. Fig. 3 shows typical TEM micrographs and electron diffraction patterns of two LPS-SiC ceramics: (a) hot-pressed at 1800 °C (LPS-SiC at 1800) and (b) hot-pressed at 1900 °C (LPS-SiC at 1900). The significant difference in characteristics between LPS-SiC at 1800 and LPS-SiC at 1900 comes from the microstructure in SiC grain size, which is much less than that of the latter. The microstructure of LPS-SiC at 1800 consisted of well-crystallized fine SiC grains (~100 nm) distribution, reflecting SiC nano-powder as a starting material. On the contrast, the microstructure of LPS-SiC at 1900 consisted of somewhat larger SiC grains (~300 nm). By electron diffraction pattern, LPS-SiC at 1900 was consistent with YAG phase (space group: *Ia3d*) as secondary phase, whose lattice constant was calculated to be 12.1 Å. Fig. 4 shows (a) STEM image and EDXS mappings of LPS-SiC at 1800 and (b) elemental analysis on the selected points in the STEM image. The microstructure revealed secondary phases, which originated from the reaction of the sintering additives. One was black phase (in STEM image) in pockets, which revealed the concentration of aluminum, yttrium and oxygen that could be speculated to be YAG. The other was an amorphous phase, which revealed the concentration of aluminum, silicon and oxygen without containing yttrium that could be speculated to be aluminum-silicate phase. The volume fraction of the crystalline YAG in LPS-SiC at 1800 was estimated to be less than 3% from XRD. The microstructure of LPS-SiC at 1900 was similar to that described above, but the amount of its amorphous phase was supposed to be much lower than that of LPS-SiC at 1800 because the volume fraction of the crystalline YAG was estimated to be about 6.8% from XRD. As shown in Fig. 5, most of the interfaces between grains were thin grain-boundary films with amorphous phase, which revealed concentration of aluminum, silicon, oxygen and yttrium, showing a width of ~20 nm.

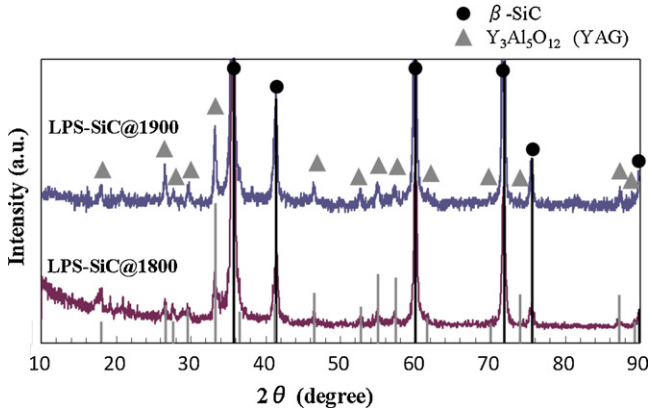

Fig. 2. X-ray diffraction profiles of two LPS-SiC ceramics.

3.2. BSR creep test

Fig. 6 shows flexural stresses in the constrained specimens, calculated from the constrained and unconstrained bend radii by Eq. (1) as a function of holding time at the test temperature. Three specimens were used to obtain the average values of flexural stress for each test temperature. In all cases, the stress exhibited a steep initial drop during 1 h, and then relaxation process was much slower by the periods. Over 3 h of holding time, the relaxation process would be saturated and the stress would be maintained.[12] In this study, maximum holding time for the BSR tests was chosen at 3 h. The initial flexural stress levels were estimated to be 43–110 MPa. Fig. 7 shows the BSR ratio (m) against the reciprocal temperatures and holding time. Three specimens were used to obtain the average m values for

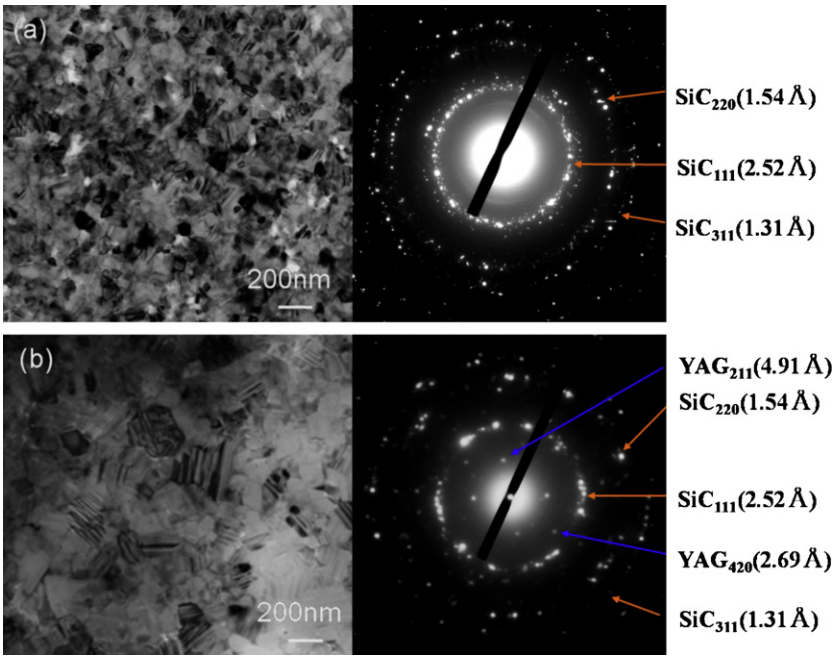

Fig. 3. Typical TEM micrographs of two LPS-SiC ceramics: (a) hot-pressed at 1800 °C (LPS-SiC at 1800) and (b) hot-pressed at 1900 °C (LPS-SiC at 1900).

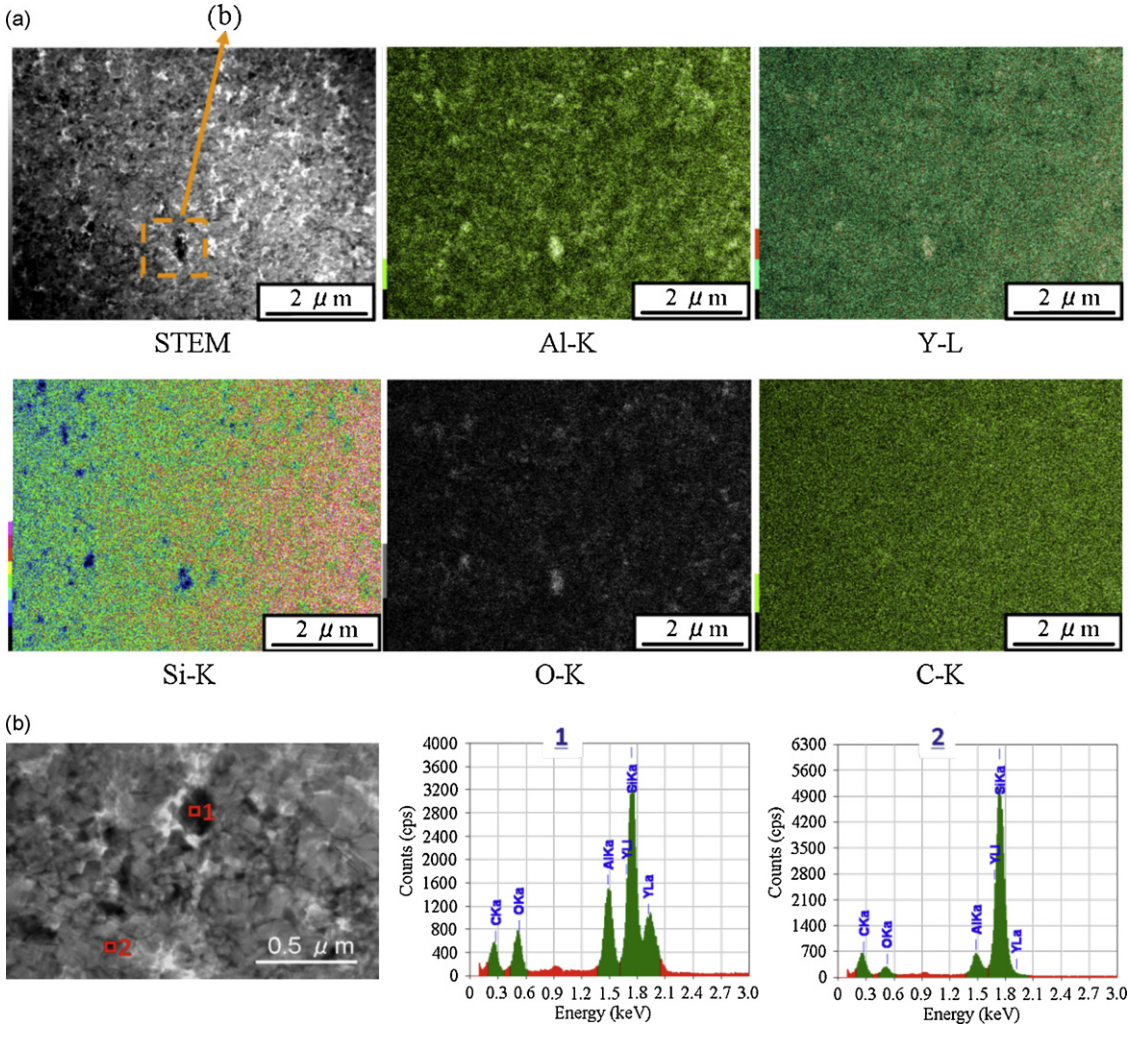

Fig. 4. STEM image and EDXS mappings at intergranular grain boundaries of LPS-SiC at 1800.

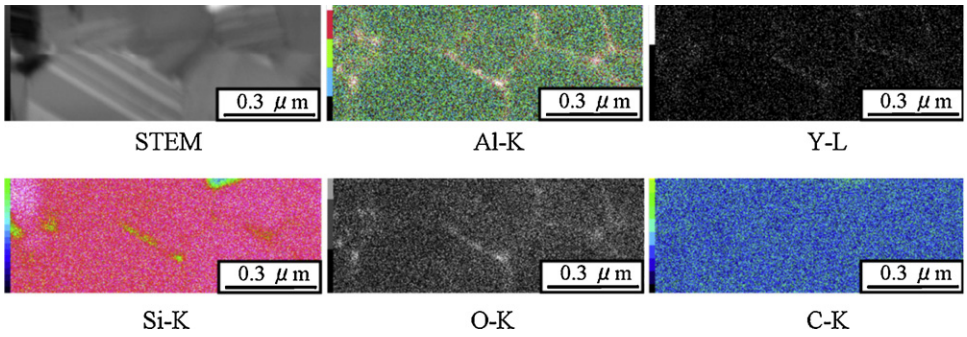

Fig. 5. (a) STEM image and EDXS mappings of LPS-SiC at 1900 when hot-pressed and (b) elemental analysis in the selected points.

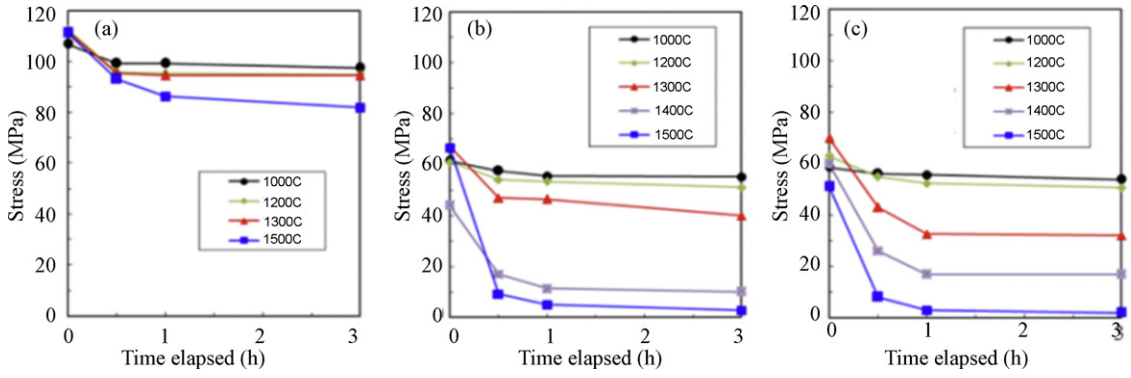

Fig. 6. Relaxation behaviors of the maximum surface stress in (a) CVD-SiC, (b) LPS-SiC at 1900 and (c) LPS-SiC at 1800 during the BSR tests.

each test temperature. Both LPS-SiC at 1800 and LPS-SiC at 1900 showed the excellent m values up to 1200 °C, which were as high as CVD-SiC with the clean grain boundaries. However, the m value of LPS-SiC at 1800 slightly decreased after the BSR test at 1300 °C by ~0.59 and rapidly decreased at 1400 °C by ~0.26. On the contrast, LPS-SiC at 1900 maintained the excellent m value over 0.80 at 1300 °C. However, the m value with the similar rapid decrease by ~0.26 occurred at 1400 °C even for LPS-SiC at 1900, which exhibited larger SiC grains in size and more crystalline YAG (less amorphous phase) when hot-pressed. Both LPS-SiC at 1800 and LPS-SiC at 1900 showed the very low m values below 0.10 at 1500 °C. CVD-SiC maintained the excellent m values by ~0.69 up to 1500 °C.

3.3. Microstructural evolutions

Fig. 8 presents (a) STEM image and EDXS mappings of LPS-SiC at 1800 at tensile edge side after the BSR test at 1300 °C for 3 h and (b) element analysis on the selected points in the STEM image. After the BSR test at 1300 °C for 3 h, a significant grain growth occurred by ~300 nm in LPS-SiC at 1800. In addition, the amorphous phase in pockets between SiC multigrains was well detectable as large clusters, which revealed the concentration of aluminum, silicon and oxygen without containing yttrium indexed to aluminum-silicate phase. The morphology and volume fraction of the black phase in pockets between SiC multigrains, which revealed the concentration of aluminum, oxygen and yttrium indexed to crystalline

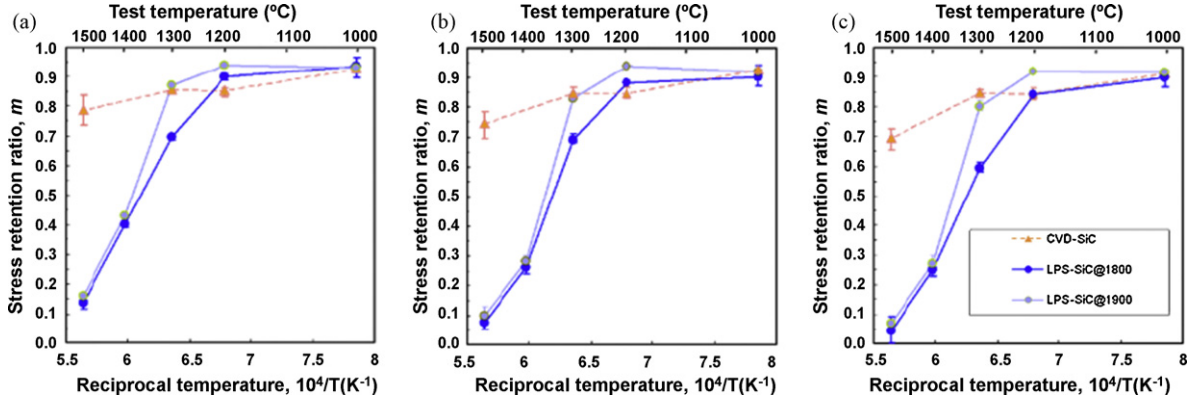

Fig. 7. Bend stress relaxation ratio (m) for CVD-SiC, LPS-SiC at 1900 and LPS-SiC at 1800 plotted against reciprocal temperatures: (a) for 0.5 h, (b) for 1 h and (c) for 3 h.

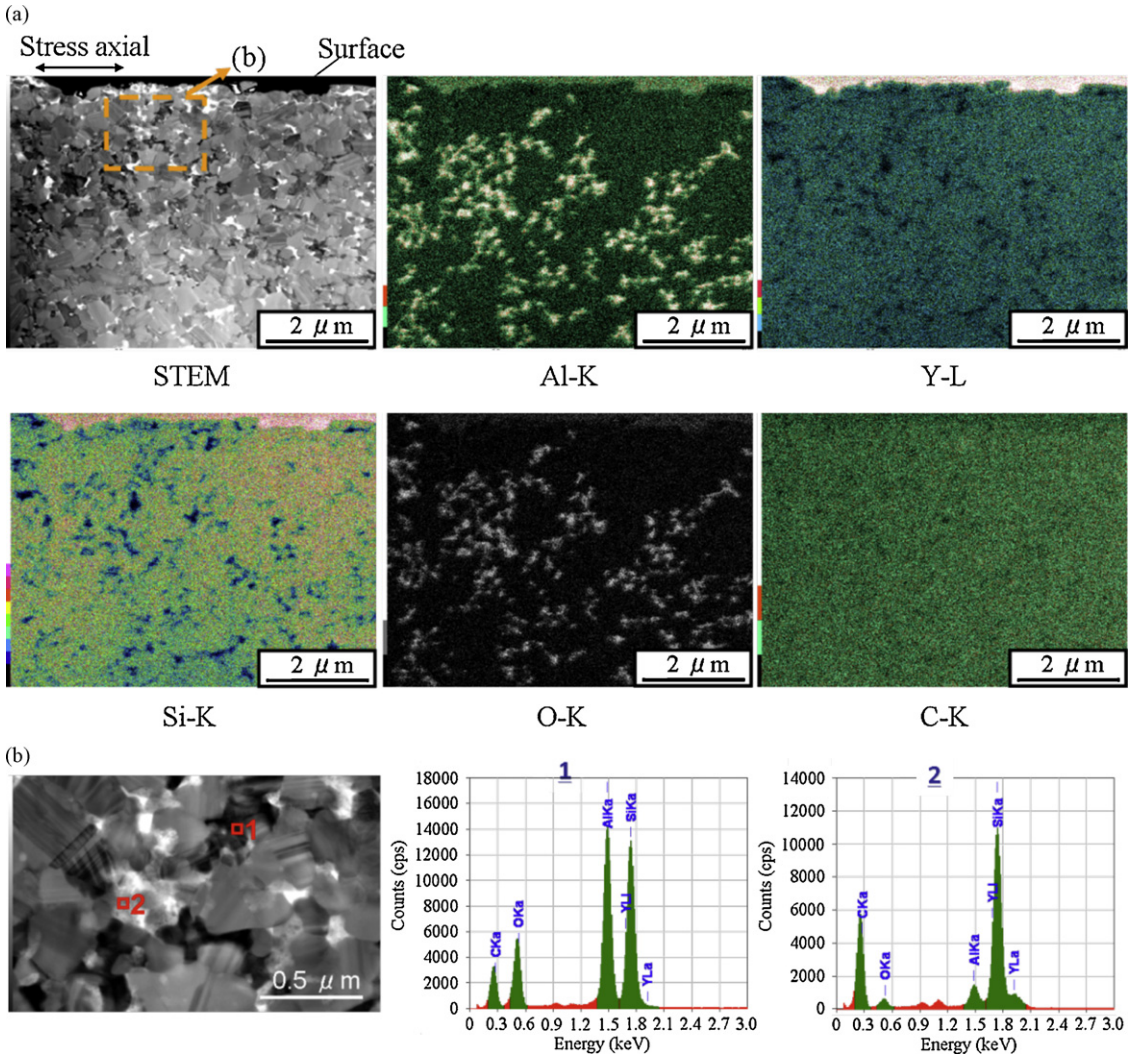

Fig. 8. (a) STEM image and EDXS mappings of LPS-SiC at 1800 at tensile edge side after the BSR test at 1300 °C for 3 h and (b) elemental analysis on the selected points.

YAG, were almost unchanged. On the contrast, the amorphous phase did not appear in large pockets between SiC multigrains in LPS-SiC at 1900, as shown in Fig. 9. Instead of such an amorphous phase, the many secondary phase, which revealed the concentration of aluminum, oxygen and yttrium indexed to crystalline YAG, were distributed as large pockets between SiC multigrains. After BSR test at 1500 °C, the BSR ratio was very low m values below 0.10 and almost thermal relaxation creep could be considered as finished for both LPS-SiC at 1800 and LPS-SiC at 1900. Fig. 10 shows (a) STEM image and EDXS mappings of LPS-SiC at 1800 at tensile edge side after the BSR test at 1500 °C for 3 h and (b) element analysis on the selected points in the STEM image. In LPS-SiC at 1800, the large pockets between SiC multigrains changed microstructure, which were well detectable as black phase (in the STEM image). The composition of the black phase revealed the concentration with aluminum, oxygen and yttrium indexed to crystalline YAG. The amorphous phase in large pockets, which was well detectable after the BSR test at 1300 °C, was completely disappeared.

4. Discussion

Creep mechanism of ceramics strongly depends on grain boundary. There are two types of grain-boundary structure in polycrystalline solids. One type is the clean grain boundary like CVD-SiC, the other is the grain boundary with amorphous films. Polycrystals with the clean grain boundaries deform by diffusional creep. Artz et al.[23] developed the theory of diffusion creep by the analyzing the movement of the boundary dislocation. The other hand, creep behavior of ceramics containing amorphous phase in pockets and at grain boundaries with thin films is completely determined by the viscous nature of the amorphous phase, the volume fraction, and the geometry of rigid grains.[24] For materials that contain a very large amount of amorphous phase (>10%), we use the expression "rheological flow" or "grain-boundary sliding accommodated by re-distribution of amorphous phase". For materials that contain a few volume fraction of amorphous phase like two LPS-SiC ceramics in this study, several simultaneous creep mechanisms will be involved. Thus, to ascribe the BSR ratio to micro-

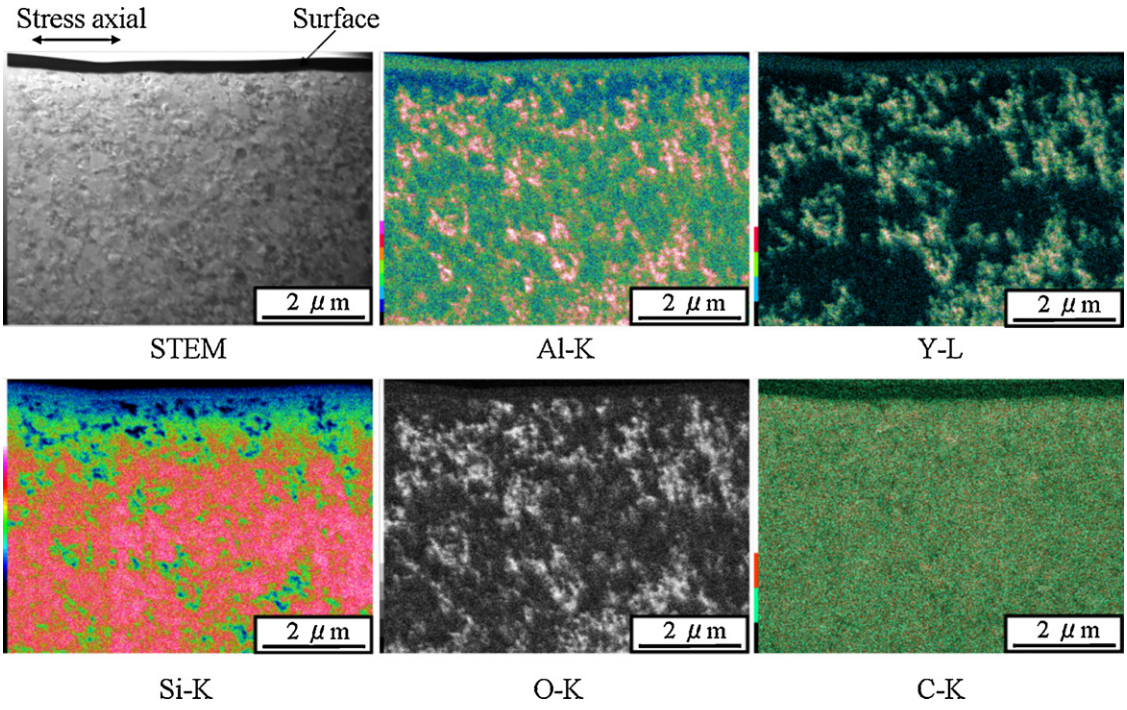

Fig. 9. STEM image and EDXS mappings of LPS-SiC at 1900 at tensile edge side after the BSR test at 1300 °C for 3 h.

scopic the creep mechanism requires a prior detailed analysis of microstructural evolutions. LPS-SiC ceramics used in this study, which consisted of nano-crystalline SiC, crystalline YAG and amorphous phases in pockets and at grain boundaries, did not reach their equilibriums because of the 'lower' fabrication temperature and short dwell time as fabricated. Therefore, the LPS-SiC ceramics underwent substantial changes in phase and microstructure during the creep tests, underlined on our observations. The m values of two LPS-SiC ceramics showed over 0.80 up to 1200 °C, which were as high as those of CVD-SiC with the clean grain boundaries. After the BSR test at 1300 °C, the m value of LPS-SiC at 1800 slightly decreased to be ∼0.59, showing the time-dependence (from 0.69 for 1 h to 0.59 for 3 h). This can be explained because of the viscous flow of the amorphous phase involving grain-boundary sliding. In Y- and Al-containing LPS-SiC ceramics utilizing submicron-powder, the plastic deformation and internal friction peak with the decrease of elastic modulus by viscous flow of the amorphous phase were commonly observed above 1000 °C.[25–27] Nanostructured LPS-SiC ceramics utilizing nano-powder is not at all an exception to that rule, or rather viscous flow in them may result in the critical creep mechanism by the enhanced grain-boundary activity from the very fine grains. Hence, the viscous flow of the amorphous phase at 1300 °C is quite starting in LPS-SiC at 1800. According to this viscous flow mechanism, the amorphous phase is squeezed out from intergranular grains under tensile tension and accumulates in multigrain pockets.[7] Consequently, the flow of the amorphous phase can explain the appearance of large pockets of amorphous phase and relatively regions of interlocked grains depleted of amorphous phase with the significant growth of SiC grains, as shown in Fig. 8. In addition, if viscous flow of the amorphous phase proceeds for a relatively long time, then one would expect the above-mentioned agglomerations to locate preferentially near the outer surface of the samples, in which they would be larger in size. By contrast, the absence of m value reduction in LPS-SiC at 1900 is much more surprising. This can be explained by the difference in microstructural evolutions between LPS-SiC at 1800 and LPS-SiC at 1900 after the BSR test at 1300 °C. Instead of the amorphous phase, the many crystalline YAG was well detectable as large pockets in LPS-SiC at 1900, as shown in Fig. 9. The size and volume fraction of the crystalline YAG was almost unchanged, compared with those of the material when hot-pressed at 1900 °C. In addition, the significant growth of SiC grains was not observed. The results from our observation indicate that this maintained m value at 1300 °C in LPS-SiC at 1900 has a close relation to the crystalline YAG content of the material when hot-pressed at 1900 °C. In other words, it could be concluded that the crystallization reduced volume fraction of the amorphous phase indexed to aluminum-silicate phase by the increase of sintering temperature remarkably increased the thermal relaxation creep resistance at 1300 °C due to preventing from viscous flow, leading to no significant time-dependence (from 0.83 for 1 h to 0.80 for 3 h). The m value of LPS-SiC at 1800 showed a significant decrease to ∼0.26 at 1400 °C, and then a further decrease below 0.10 at 1500 °C. Simultaneously, the amorphous alumina-silicate phase was disappeared and crystalline YAG was formed at 1500 °C. This YAG formation involving the disappearance of the amorphous phase should take the responsibility of the significant decrease against the BSR creep resistance. This YAG crystallization has been identified during creep of LPS-SiC ceramics using electron energy-loss spectroscopy (EELS) by Gu et al.[22] To form YAG phase, the Al:Y ratio must be reduced to 5:3. In other words, Al content in the amorphous pockets should decrease and Y con-

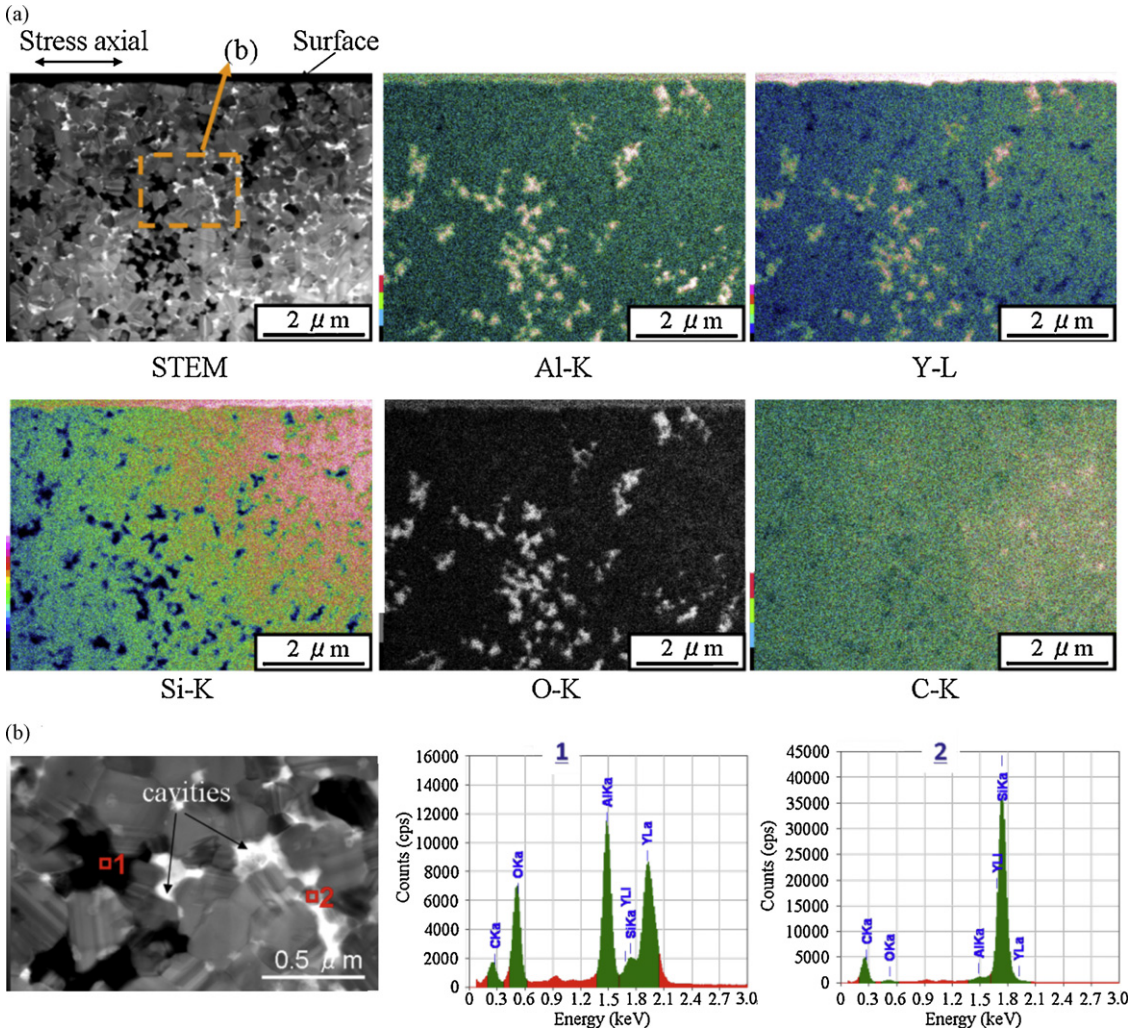

Fig. 10. (a) STEM image and EDXS mappings of LPS-SiC at 1800 at tensile edge side after the BSR test at 1500 °C for 3 h and (b) elemental analysis on the selected points.

tent should increase. This compositional change would require Al content in grain-boundary films to increase and Y content to decrease, since these additives did not solid solution in SiC grains. The increase of Al content in grain boundary during creep is probably occurred,[22,28] although such compositional analysis at grain boundaries is not performed in the present study. Thus, it is reasonably explained to think that the inter-diffusion of Al–Y among intergranular regions is dominating atomic diffusion process during the creep above 1400 °C. Although it has been pointed the opposite out elsewhere, our empirical results demonstrated that the applicability of nanostructured LPS-SiC ceramics containing crystalline YAG as a structural material is not restricted to the temperature below 1345 °C ternary eutectic temperature.[29] After the BSR test at 1500 °C, some cavities in pockets were observed in two LPS-SiC ceramics, as shown in Fig. 10(b). LPS-SiC ceramics might undergo chemical transformations at high temperatures required for creep. The evaporation of the amorphous phase has been usually attributed to SiO volatilization in LPS-SiC ceramics. The amorphous phase in pockets and at grain boundaries is continuous path for fast diffusion of gaseous molecules.[24] The low viscosity of the amorphous phase with the ternary eutectic composition enhances the evaporation. In addition, yttrium aluminates ($Y_3Al_5O_{12}$ (YAG), $YAlO_3$ (YAP), $Y_4Al_9O_{12}$ (YAM)) have been shown to decompose in the presence of SiC at high temperatures. Indeed, Mah et al.[21] reported that YAG was highly stable at up to 1650 °C in air and under vacuum, but underwent sever decomposition at temperature as low as 1500 °C under vacuum in the presence of SiC. In their opinions, the decomposition of YAG was accompanied by the formation of aluminum-containing gaseous species with the reactions between YAG and gaseous CO, resulting in the decrease of Al content.[7,14,21] The source of gaseous CO is sufficiently produced by the active oxidation of SiC under low oxygen partial pressure:

$$SiC(s) + O_2(g) = SiO(g) + CO(g) \quad (3)$$

The validation of the above argument was confirmed by the decrease of Al content after the BSR test at 1500 °C using EDXS for both LPS-SiC at 1800 and LPS-SiC at 1900. The formation of volatile species from the amorphous phase and the carbothermal reduction of crystalline YAG might be at the origin of the observed extensive nucleation and spectacular growth of cavi-

ties, as shown in Fig. 10. In short, the *m* values of LPS-SiC at 1900, which contained larger grains in size and less amorphous phase by crystallization of YAG, were supposed to be as low as those of LPS-SiC at 1800 above 1400 °C.

In nanostructured LPS-SiC ceramics, a few volume fraction of amorphous phase in pockets and at grain boundaries would affect thermal stress relaxation creep, as previously described. In particular, the differences of crystalline YAG (or amorphous phase) content as secondary phase in the LPS-SiC ceramics when hot-pressed had a significant effect on the creep resistance. The observed thermal relaxation creep seems to result from the contribution of a set of simultaneous and/or concurrent processes (grain-boundary sliding + viscous flow of the amorphous phase + chemical transformation of YAG + formation and growth of cavities). In spite of the obvious difficulties associated with the identification of the thermal relaxation creep mechanisms, and from the viewpoint of the possible structural applications of the LPS-SiC ceramics, it should be noted that the two materials exhibit relatively good creep characteristics up to 1200 °C. The suitability of nanostructured LPS-SiC ceramics containing crystalline YAG is thus demonstrated for the nuclear applications, such as gas-cooled fast reactors and fusion reactors, in which the maximum operating temperatures are estimated under 1200 °C.[2–4]

5. Conclusions

The thermal stress relaxation creep characteristics of nanostructured LPS-SiC ceramics by hot-pressing at 1800 or 1900 °C was investigated using BSR method. The creep behaviors were strongly related to the microstructure evolutions during the creep due to the reach under their equilibriums when hot-pressed. The creep was characterized by the BSR ratio of ∼0.8 up to 1200 °C, and the volume fraction of crystalline YAG (or amorphous phase) in the materials was associated to the creep resistance at 1300 °C. The microstructural evolutions during the creep of the LPS-SiC ceramics consisted in firstly the re-distribution of the amorphous phase, probably as a consequent of viscous flow, and of secondly the extensive nucleation and growth of cavities. The former furthermore enhanced inter-diffusion of Al–Y among intergranular regions above the ternary eutectic temperature of 1345 °C, which caused the significantly reduced creep resistance for both materials. The latter reflected the carbothermal reduction of crystalline YAG involving the decrease of Al content, which was the reaction between crystalline YAG and gaseous CO. Our demonstrative finding can be thought of as a suitability of nanostructured LPS-SiC ceramics containing crystalline YAG for the nuclear applications, in which maximum operating temperatures are estimated under 1200 °C.

Acknowledgements

This work was partly supported by "Innovative Nuclear Energy System Technology" program, funded by the Ministry of Education, Culture, Sports, Science and Technology (MEXT), Japan.

References

1. Dapkunas SJ. Ceramic heat exchangers. *Am Ceram Soc Bull* 1988;**67**(2):388–91.
2. Naslain R. Design, preparation and properties of non-oxide CMCs for application in engines and nuclear reactors: an overview. *Compos Sci Technol* 2004;**64**(12):155–70.
3. Kohyama A. Advanced SiC/SiC composite materials for fourth generation gas cooled fast reactors. *Key Eng Mater* 2005;**287**:16–21.
4. Riccardi B, Giancarli L, Hasegawa A, Kohyama A, Jones RH, Snead LL. Issues and advances in SiC_f/SiC composites development for fusion reactors. *J Nucl Mater* 2004;**329–333**(1):56–65.
5. Gallardo-Lopez A, Munoz A, Martinez-Fernandez J, Dominguez-Rodriguez A. High-temperature compressive creep of liquid phase sintered silicon carbide. *Acta Mater* 1999;**47**(7):2185–95.
6. Castillo-Rodriguez M, Munoz A, Dominguez-Rodriguez A. Correlation between microstructure and creep behavior in liquid-phase-sintered alpha-silicon carbide. *J Am Ceram Soc* 2006;**89**(3):960–7.
7. Melendez-Martinez JJ, Castillo-Rodriguez M, Domiguez-Rodriguez A, Ortiz AL, Guiberteau F. Creep and microstructural evolutions at high temperature of liquid-phase-sintered silicon carbide. *J Am Ceram Soc* 2007;**90**(1):163–9.
8. Morcher GN, Pujar VV. Creep and stress–strain behavior after creep for SiC fiber reinforced, melt-infiltrated SiC matrix composites. *J Am Ceram Soc* 2006;**89**(5):1652–8.
9. Pezzotti G, Kleebe HJ. Grain-boundary relaxation in high-purity silicon nitride. *J Am Ceram Soc* 1996;**79**(9):2237–46.
10. Lin HT, Breder K. Creep deformation in an alumina–silicon carbide composite produced via a directed metal oxidation process. *J Am Ceram Soc* 1996;**79**(8):2218–20.
11. Morscher GN, Dicarlo JA. A simple test for thermomechanical evaluation of ceramic fibers. *J Am Ceram Soc* 1992;**75**(1):136–40.
12. Katoh Y, Snead LL. Bend stress relaxation creep of CVD silicon carbide. *Ceram Eng Sci Proc* 2005;**26**(2):265–72.
13. Katoh Y, Snead LL, Hinoki T, Kondo S, Kohyama A. Irradiation creep of high purity CVD silicon carbide as estimated by the bend stress relaxation method. *J Nucl Mater* 2007;**367–370**(1):758–63.
14. Shimoda K, Eiza N, Park JS, Hinoki T, Kohyama A, Kondo S. High-temperature mechanical property improvements of SiC ceramics by NITE process. *Mater Trans* 2006;**47**(4):1204–8.
15. Ohyanagi M, Yamamoto T, Kitaura H, Kodera Y, Ishii T, Munir ZA. Consolidation of nanostructured SiC with disorder–order transformation. *Scripta Mater* 2004;**50**(1):111–4.
16. Lee YI, Kim YW, Mitomo M, Kim DY. Fabrication of dense nanostructured silicon carbide ceramics through two-step sintering. *J Am Ceram Soc* 2003;**86**(10):1803–5.
17. Shimoda K, Park JS, Hinoki T, Kohyama A. Influence of surface structure of SiC nano-sized powder analyzed by X-ray photoelectron spectroscopy on basic powder characteristics. *Appl Surf Sci* 2007;**253**(24):9450–6.
18. Shimoda K, Park JS, Hinoki T, Kohyama A. Densification mechanism and microstructural evolutions of SiC matrix in NITE process. *Ceram Eng Sci Proc* 2006;**27**(5):19–27.
19. Kim JY, Kim YW, Mitomo M. Microstructure and mechanical properties of alpha-silicon carbide sintered with yttrium–aluminum garnet and silica. *J Am Ceram Soc* 1999;**82**(2):441–4.
20. Cheong DI, Kim JS, Kang SL. Effects of isothermal annealing on the microstructure and mechanical properties of SiC ceramics hot-pressed with Y_2O_3 and Al_2O_3 additions. *J Eur Ceram Soc* 2002;**22**(8):1321–7.
21. Mah TI, Keller KA, Sambasivan S, Kerans RJ. High-temperature environmental stability of the compounds in the Al_2O_3–Y_2O_3 system. *J Am Ceram Soc* 1997;**80**(4):874–8.
22. Gu H, Nagano T, Zhan GD, Mitomo M, Wakai F. Dynamic evolutions of grain-boundary films in liquid-phase-sintered ultrafine silicon carbide material. *J Am Ceram Soc* 2003;**86**(10):1753–60.
23. Artz E, Ashby MF, Verral RA. Interface controlled diffusional creep. *Acta Metall* 1983;**31**(12):1977–89.

24. Wakai F, Kondo N, Ogawa H, Nagano T, Tsurekawa S. Ceramics superplasticity: deformation mechanisms and microstructures. *Mater Charact* 1996;**37**(5):331–41.
25. Biswas K, Rixeckera G, Aldinger F. Creep and visco-elastic behaviour of LPS-SiC sintered with Lu_2O_3–AlN additive. *Mater Chem Phys* 2007;**104**(1):10–7.
26. Roebben G, Van der Biest O, Sciti D, Bellosi A, Sarbu C, Lauwagie T. High-temperature stiffness and damping measurements to monitor the glassy intergranular phase in liquid-phase-sintered silicon carbides. *J Am Ceram Soc* 2005;**88**(8):2152–8.
27. Roebben G, Duan RG, Sciti D, Van der Biest O. Assessment of the high temperature elastic and damping properties of silicon nitrides and carbides with the impulse excitation technique. *J Eur Ceram Soc* 2002;**22**(14–15):2501–9.
28. Zhang XF, Sixta ME, De Johghe LC. Grain boundary evolutions in hot-pressed ABC-SiC. *J Am Ceram Soc* 2000;**83**(11):2813–20.
29. Jensen RP, Luecke WE, Padture NP, Wiederhorn SM. High-temperature properties of liquid-phase-sintered α-SiC. *Mater Sci Eng A* 2000;**282**(1–2):109–14.